

# 1 **Bidirectional FtsZ filament treadmilling transforms lipid membranes via torsional stress**

2 **Authors:** Diego A. Ramirez-Diaz<sup>1,2</sup>, Adrian Merino-Salomon<sup>1,3</sup>, Fabian Meyer<sup>5</sup>, Michael  
3 Heymann<sup>1</sup>, German Rivas<sup>4</sup>, Marc Bramkamp<sup>5</sup> & Petra Schwille<sup>1\*</sup>.

## 4 **Affiliations:**

5 <sup>1</sup>.Department of Cellular and Molecular Biophysics, Max Planck Institute for Biochemistry,  
6 Martinsried, Germany

7 <sup>2</sup>.Graduate School for Quantitative Biosciences (QBM), Ludwig-Maximilians-University,  
8 Munich, Germany

9 <sup>3</sup>.International Max Planck Research School for Molecular Life Sciences (IMPRS-LS), Munich,  
10 Germany.

11 <sup>4</sup>.Centro de Investigaciones Biologicas, Consejo Superior de Investigaciones Cientificas  
12 (CSIC), Madrid, Spain.

13 <sup>5</sup>.Institute of Microbiology, Christian-Albrechts-University, Kiel, Germany.

14

15 **Abstract:** FtsZ is a key component in bacterial cell division, being the primary protein of the  
16 presumably contractile Z ring. *In vivo* and *in vitro*, it shows two distinctive features that could  
17 so far however not be mechanistically linked: self-organization into directionally treadmilling  
18 vortices on solid supported membranes, and shape deformation of flexible liposomes. In cells,  
19 circumferential treadmilling of FtsZ was shown to recruit septum-building enzymes, but an  
20 active force production remains elusive. To gain mechanistic understanding of FtsZ dependent  
21 membrane deformations and constriction, we designed an *in vitro* assay based on soft lipid  
22 tubes pulled from FtsZ decorated giant lipid vesicles (GUVs) by optical tweezers. FtsZ actively  
23 transformed these tubes into spring-like structures, where GTPase activity promoted spring

24 compression. Operating the optical tweezers in lateral vibration mode and assigning spring  
25 constants to FtsZ coated tubes, we found that FtsZ rings indeed exerts 0.14 – 1.09 pN forces  
26 upon GTP hydrolysis, through torsional stress induced by bidirectional treadmilling. These  
27 directional forces could further be demonstrated to induce membrane budding with constricting  
28 necks on both, giant vesicles and *E.coli* cells devoid of their cell walls.

29  
30 **Main Text:** In biology, fundamental mechanical processes, such as cell division, require an  
31 intricate space-time coordination of respective functional elements. However, how these  
32 elements, mostly proteins, can self-organize to exert forces driving large-scale transformations  
33 is poorly understood. In several organisms, ring-like cytoskeletal elements appear upon  
34 cytokinesis; for instance, the FtsZ-based contractile Z ring in bacteria. Ring-like FtsZ structures  
35 have previously been shown to deform liposome membranes (1,2). When reconstituted on flat  
36 membranes, FtsZ self-assembles into rotating-treadmilling vortices with conserved direction  
37 (3,4). *In vivo*, FtsZ shows circumferential but bidirectional treadmilling that is assumed to serve  
38 as a pacemaker guiding peptidoglycan synthesis around the septum (5,6).

39  
40 Despite of these exciting findings, it is not clear whether these treadmilling FtsZ filaments  
41 actively contribute to the physical process of lipid membrane constriction and cytokinesis in  
42 bacteria (7,8). The challenge is two-fold: (i) how much force is actually required to divide  
43 bacteria, given the mechanical coupling of the lipid membrane and the cell wall?, and (ii) even  
44 if FtsZ filaments can generate membrane deforming forces, what is the exact mechanism by  
45 which these forces are exerted? For instance, considering the mechanical bearing related to  
46 internal turgor pressure (~MPa), models have suggested that FtsZ forces in the range of 8-80  
47 pN would be required for constriction (9). In contrast, it has been proposed that turgor pressure  
48 need not be considered, due to the possibility of same osmolarity between periplasm and  
49 cytoplasm (10). For this case, very low FtsZ forces in the range of 0.35 – 2.45 pN could exert

50 membrane deformations leading to constriction (10). In conclusion, *in vivo* and *in vitro*  
51 experimental approaches addressing those two major questions are needed to gain deeper  
52 understanding in cell division in bacteria.

53  
54 Here, we have employed *in vitro* reconstitution as a strategy to understand the mechanistic  
55 features of FtsZ as a membrane deforming polymer. Using an optical tweezers-based approach  
56 by pulling soft lipid tubes from deflated giant unilamellar vesicles GUVs, our aim is to  
57 quantitatively elucidate the physical principles underlying membrane deformations induced by  
58 dynamic FtsZ rings on GUVs and the scale of delivered forces. These particular principles are  
59 key to understand the nature of FtsZ membrane deformations *in vitro* and *in vivo*.

60  
61 Based on our recent study (3), we externally added FtsZ-YFP-mts to GUVs made of *E. coli*  
62 lipid extract. Conditions to obtain ring-like structures were determined by tuning GTP and  $Mg^{+2}$   
63 (Fig. 1A). Since no clear deformations were observed for tensed vesicles (Fig. 1A), we designed  
64 a two-side open chamber allowing for slow water evaporation to obtain deflated and deformable  
65 GUVs. After 20-30 minutes, we evidenced that rings were inducing inwards-cone structures  
66 emerging from the membrane surface, indicative of drilling-like inward forces (Fig. 1B).  
67 Motivated by this specific geometry, we designed PDMS microstructures mimicking such  
68 inward cones (Fig. 1C Fig 1SA). After coating these with supported lipid bilayer (SLB) and  
69 triggering protein polymerization, we observed individual filaments/bundles to wrap the cone  
70 in a dynamic fashion resembling a vortex (Fig. 1D) (Movie S1). We noticed that the dynamic  
71 vortices rotate both clockwise and anticlockwise (Fig. 1E), indicating that preferential  
72 directionality observed on flat SLBs is absent in conical geometry. Rotational velocities were  
73 estimated around 43 *nm/s*, showing relatively good agreement with our previous results on  
74 flat surfaces (34 *nm/s*) (3).

75

76 To quantitatively characterize the impact of FtsZ on soft tubular geometries, we developed a  
77 method based on optical tweezers. Contrary to prior approaches using micropipettes (11), we  
78 pulled soft tubules from weakly surface-attached GUVs (Fig. 2SA) by moving the GUVs  
79 relative to an optically trapped bead. Lipid tubes with mean diameter of ca.  $0.47 \mu\text{m}$  (Fig. 2SB)  
80 were now pulled from deflated GUVs decorated with ring-like FtsZ structures and inward-  
81 conical deformations (Movie S2). Once tubes were formed, protein filaments entered and  
82 deformed the tube. After 175s, helical tube shapes were clearly observed (Fig. 2A), indicative  
83 of dynamic coiling (Movie S3). As more protein entered the tube and accumulated in the tip,  
84 the spring-like structure got compressed (Fig. 2A, 500s). These helical tube deformations can  
85 be rationalized by twisting of an elastic rod subjected to constant tensile force (Fig. 3F). Similar  
86 to the experiment in Figure 1D, filaments grew towards (clockwise) and away from  
87 (counterclockwise) the tip of the tube. If filament growth imposes torsion, the counter-growing  
88 filament will generate torsion in the opposite direction. These two different torsional  
89 contributions result in the buckling of the lipid tube and the formation of a 3D helix (Fig. 3F).  
90 The importance of the bidirectional treadmilling, or bidirectional filament growth, can be  
91 understood using a shoelace analogy: opposite torque should be exerted on both ends of the  
92 shoelace to observe a helical deformation. If one end is loose, the opposite end will only rotate  
93 accordingly (sliding). A net force due to FtsZ twisting and coiling in the outwards-vesicle  
94 direction caused the incorporation of new lipid material from the flaccid vesicle to the tube.  
95  
96 Since spring-like deformations were observed with a FtsZ protein chimera that binds  
97 autonomously to membrane (FtsZ-YFP-mts), we attempted to confirm whether this  
98 phenomenology is intrinsic to the FtsZ polymer and not caused by the membrane targeting  
99 sequence. Based on the reconstitution of dynamic rings on flat membranes using the *E. coli* FtsZ  
100 natural anchor ZipA (12), we identified the right conditions to obtain WT-FtsZ rings externally  
101 decorating GUVs using ZipA (Fig. 2B). In the same way as for FtsZ-YFP-mts, rings induced

102 inwards cone-like deformations on deflated vesicles (Fig. 2B). The obvious next step was to  
103 evaluate their impact on a soft tubular geometry. As a control, we pulled lipid tubes having only  
104 ZipA to evidence missing deformation. Then we added WT-FtsZ and observed helical  
105 transformations as expected (Fig. 2B), indicating that FtsZ polymer and not its membrane  
106 attachment caused this effect. Interestingly, FtsZ-YFP-*mts* as well as FtsZ+ZipA displayed in  
107 plectonic/supercoiled regions (Fig. 1SE) as further indicative of torsion over the lipid tube.

108  
109 To investigate the role of GTP hydrolysis, we reconstituted FtsZ-YFP-*mts*\*[T108A], a mutant  
110 with low GTPase activity (3). We observed that FtsZ-YFP-*mts*\*[T108A] also self-assembled  
111 into ring-like structures (Fig. 1SB) that lacked dynamic treadmilling (3) yet still promoted  
112 inwards deformations (Fig. 1SC). Interestingly, the activity of FtsZ-YFP-*mts*\*[T108A] on the  
113 tubes was much delayed (Fig. 2SC). Although helical deformations were also observed after  
114 350s (Fig. 3B), their pitch remained considerably longer ( $\lambda > 3 \mu m$ ) also at long times (900s).  
115 In contrast, helices decorated with GTP-active FtsZ-YFP-*mts* (Fig. 3A) underwent compression  
116 to a pitch of  $\lambda \sim 1.5 \mu m$  after 300s. By plotting the arc-length of the spring against FtsZ  
117 density on the tube, we clearly observed a greater membrane-deforming activity for FtsZ-YFP-  
118 *mts* (Fig. 2SE). Experiments shown in Fig. 3A-B correspond to similar tube diameters ( $d = 0.44$   
119  $\mu m$  Fig. 2SB).

120  
121 Since the deflation of individual GUVs could vary, we also tested whether compression could  
122 be biased by GUV membrane tension (deflation) and protein density over the tube. The tube  
123 diameter  $d$  represented our observable for membrane tension according to the relation  $d = \sqrt{\frac{2\kappa}{\sigma}}$ ,  
124 where  $\kappa$  denotes the lipid bending modulus and  $\sigma$  the membrane tension (11,13). The lower the  
125 membrane tension (deflation), the larger the tube diameter. Therefore, we plotted the mean  
126 pitch vs tube diameter (Fig. 3C), for independent experiments, considering also the amount of

127 protein (Fig. 3D). Although there was a mild correlation between pitch and diameter (Fig. 3C)  
128 for FtsZ-YFP-mts, the mean pitch was consistently longer for FtsZ-YFP-mts\*[T108A] (Fig.  
129 3C) in the case of tubes with comparable or higher protein density (Fig. 3D). To better visualize  
130 the impact of GTPase activity, we plotted the pitch distribution for both proteins: the GTPase  
131 activity contributed to a decrease of pitch (Fig. 3E) as clear indicative of spring compression.  
132 Interestingly, both distributions are reasonably bimodal, indicative of two states of torsion: a  
133 structural intrinsic torsion (longer pitch) that is further enhanced (shorter pitch) via GTPase  
134 activity (Fig. 3F). Note that FtsZ-YFP-mts\*[T108A] could exhibit residual GTPase activity  
135 driving some compression.

136  
137 To quantitatively characterize the mechanical properties of FtsZ-YFP-mts-induced spring-like  
138 structures, we implemented an alternative approach based on the elastic response of the GUV  
139 + tube to a specific dynamic input. Using a piezoelectric stage, we induced a lateral oscillation  
140 of the GUV position ( $A = 3 \mu m$ ,  $f = 1 Hz$ ) and recorded forces by the optical trap (Movie S4).  
141 We here measured the resistive force of the material per micrometer (k-spring constant). The  
142 stiffer the material, the higher force detected by the optical trap. To calculate the amplitude of  
143 the signal at 1 Hz the signal was Fast Fourier Transformed, as depicted in Figure 4B, where the  
144 red line refers to the pure lipid tube and the green line to lipid + FtsZ. Due to variability in terms  
145 of vesicle size, deflation state and FtsZ surface concentration, a range of values was here  
146 reported rather than a normal-distribution. The pure lipid contribution (N=11) had values  
147 between  $0.15 - 0.55 \text{ pN}/\mu m$  (Fig. 4C), while for the lipid + FtsZ system (Fig. 4A) (N=36) we  
148 determined values between  $0.23 - 1.52 \text{ pN}/\mu m$  (Fig. 4C). Note that for some vesicles, the pure  
149 lipid response yet dominated the spring constant measurement. Based on these results, we next  
150 attempted to estimate the range of forces that a single FtsZ ring delivered. To this end, the FtsZ  
151 fluorescence signal per single ring was determined and compared to the signal on the FtsZ-  
152 covered tubes (Fig. 2SF). Thus, for each force measurement we were able to approximate the

153 “number of rings” according to the total FtsZ brightness. By plotting these forces vs “number  
154 of rings” (Fig. 4D), we noted that scattered data can be well described by two straight lines, and  
155 consequently their slopes defined the range of forces per ring: 0.14-1.09 pN.

156

157 Interestingly, we had previously inferred that FtsZ-YFP-mts rings on SLB are made of filaments  
158 of  $\sim 0.39 \mu\text{m}$  in average (3). This estimation could be used to validate our force measurements.

159 A FtsZ filament with a persistence length  $\sim 0.39 \mu\text{m}$  exhibits a flexural rigidity  $K =$   
160  $1.59 \times 10^{-27} \text{ Nm}^2$  that agrees well with Turner et. al., (2012) (14). Based on this, we could

161 calculate the Young’s modulus of FtsZ filaments:  $E_{FtsZ} = 51.8 \text{ MPa}$ . ( $E = KI$  where  $I =$   
162  $\pi r^4/4$ , the area moment of inertia,  $r = 2.5 \text{ nm}$  (15)). On the other hand, the Young’s modulus

163  $E$  of a spring is related to the spring constant through  $E = (k l_0)/S$ , where  $k$  denotes the spring  
164 constant,  $l_0$  is the spring initial length and  $S$  the cross-section. Since  $l_0/S$  was fairly constant in

165 our tube experiments, we could claim that  $E_{FtsZ}/E_l = (k_{FtsZ}/k_l)$ . To calculate  $\frac{k_{FtsZ}}{k_l}$ , we here  
166 considered raw averages for distributions shown in Fig. 4C and subtracted the lipid contribution

167 in the case of FtsZ:  $k_l = 0.34 \text{ pN}/\mu\text{m}$  and  $k_{FtsZ} = 0.6 \text{ pN}/\mu\text{m}$ . Then, the ratio  $\frac{k_{FtsZ}}{k_l} = 1.76$

168 showed good agreement compared to  $\frac{E_{FtsZ}}{E_l} = 2.26$  assuming  $E_l = 22.9 \text{ MPa}$  (lipids with

169 bending  $\kappa = 20 k_b T$ ) (16, 17). This confirmed that our force measurements corresponded well

170 with previous flexural rigidity values for FtsZ fibers. In addition, our data provide further

171 evidence that FtsZ filaments are softer than other cytoskeleton proteins such as microtubules

172 ( $K \sim 10^{-23}$ ) or actin ( $K \sim 10^{-26}$ ) (18,19)

173

174 The helical nature of FtsZ and its torsional dynamics have been experimentally observed (20,

175 21); however, its relation to a potential mechanism of deforming membranes has not yet been

176 clearly established. According to our observations, the helical membrane transformation caused

177 in this study by FtsZ filaments can best be understood by assuming Darboux torque around the

178 lipid tube. Darboux torques are tangential torques caused by a local mismatch between the plane  
179 defined by the filament curvature and the membrane attachment direction (22). This twisting  
180 angle along the one filament is key to produce torque. A molecular dynamics study showed that  
181 dynamin, a helical endocytic constriction protein, required twisting of the “adhesive-stripe” to  
182 achieve full membrane hemifusion (22). In the case of FtsZ, molecular dynamics studies have  
183 predicted an angle of “twisting” along the c-terminus, where membrane attachment occurs (23,  
184 24). Also, Fierling and coworkers have theoretically studied membrane deformations produced  
185 by filaments inducing torques (25). Strikingly, they found inward vortex-like deformations  
186 from flat surfaces and spring-like shapes when filaments wrapped around a tubular geometry  
187 (25). These predictions agree remarkably well with our observations.

188  
189 So far, we had investigated an inverse geometry, i.e., FtsZ added from the outside, as compared  
190 to the physiological case. Now we also reconstituted FtsZ-YFP-mts and FtsZ-YFP-  
191 mts\*[T108A] inside GUVs (Fig. 5A). Conditions to obtain ring-like-structures (Fig. 5B) or  
192 filaments wrapping the vesicle (Fig. 1SD) were again found by tuning GTP and  $Mg^{+2}$ .  
193 Interestingly, the diameters of FtsZ-YFP-mts\*[T108A] rings were significantly larger  
194 ( $0.89 \mu m$ ) than FtsZ-YFP-mts ( $0.44 \mu m$ ) (Fig. 5D). This difference was not observed in the  
195 case of SLBs (3), indicating the possibility that softer lipid surface affects the steady state of  
196 FtsZ assembly. In other words, the physical properties of the lipid surface, such as stiffness,  
197 may play an important role in FtsZ fragmentation and treadmilling. In addition, the wide size  
198 distribution in the low GTPase mutant case (Fig. 5D) implied that polymers were flexible to  
199 accommodate a larger variety of curvatures. Strikingly, both FtsZ mutants could create  
200 outwards deformations emerging from rings (Fig. 4E). But only in the case of FtsZ-YFP-mts,  
201 there was clear evidence of constricting rings (Fig. 4E) similar to previous reports (1). Based  
202 on Fig. 1, we hypothesize that FtsZ torsion could create outwards out-of-plane forces (Fig. 5F).  
203 However, FtsZ filaments only exhibiting static (structural) torsion were unable to stabilize



204 smaller diameters. In contrast, dynamic twisting upon GTP-hydrolysis drives constriction and  
205 clustering (Fig. 5G), such that active FtsZ filaments lead to an overall shrinkage of diameters.  
206 FtsZ constriction and neck formation on flat membranes thus represents an analog of helix  
207 compression, where forces of 0.14 – 1.09 pN per ring are actuating the lipid surface.

208  
209 In order to appreciate the relevance of our mechanistic findings for lipid membranes *in vivo*,  
210 we needed to transfer our FtsZ-YFP-mts construct to the cellular environment. Therefore, *E.*  
211 *coli* cells were cloned and transformed with the corresponding gene into an inducible plasmid.  
212 Upon IPTG induction, FtsZ-YFP-mts fluorescence signals in the cells were observed. The FtsZ-  
213 YFP-mts construct localizes in several ring-like structures around midcell (Fig. 6A). Multiple  
214 Z-ring structures were observed, due to the overexpression of the FtsZ-YFP-mts protein (1). A  
215 3D-reconstruction reveals that these FtsZ assemblies are indeed ring structures that resemble  
216 those formed by native FtsZ rings at the division site (Fig. 6A). Importantly, without addition  
217 of inductor, no FtsZ-YFP-mts structures were observed (Fig. 6B). Since FtsZ driven  
218 deformations were not observed for tensed GUVs (Fig. 5), we reasoned that in walled bacteria  
219 with turgor pressure, it might be difficult to observe FtsZ-YFP-mts driven membrane  
220 deformations. Therefore, cells were treated with lysozyme to create *E. coli* spheroplasts in  
221 osmoprotective medium. Cells expressing the FtsZ fusion protein were highly fragile and prone  
222 to lysis. We therefore started microscopic analyses before all cells have converted to  
223 spheroplasts (Fig. 6B). Importantly, vesicular structures budding out from spheroplasted cells  
224 were observed (Fig. 6B, arrows). These vesicular structures were not observed in control cells  
225 lacking the FtsZ-YFP-mts expression, indicating that they are a consequence of protein  
226 overproduction. We also observed drastic deformations of the plasma membrane that resemble  
227 plasmolysis. In these cases, FtsZ-YFP-mts assemblies underneath the membrane seem to pull  
228 in the membrane and exert force leading to a separation of plasma membrane and outer  
229 membrane. A membrane stain reveals that areas with strong FtsZ fusion protein assemblies also

230 show membrane invaginations or constriction necks (Fig. 6C, arrows; Movie S5). These results  
231 agreed remarkably well with our outwards deformations and constriction necks from FtsZ rings  
232 inside GUVs. Directional screw-like forces promoting extrusion of lipid material or budding  
233 (Fig. 5H & Fig. 6B), as well as constriction necks (Fig. 5G & Fig. 6C), are both explained in  
234 terms of a FtsZ polymer able to exert torsional stress as explained above. Interestingly, this  
235 opens the possibility of FtsZ filaments playing an active role in cell division organisms that  
236 divide by budding, such as *Acholeplasma laidlawii* (28).

237  
238 Altogether, our experiments provide clear evidence that FtsZ induces two kinds of mechanical  
239 deformations to membranes. Static (structural) FtsZ torsion rules the assembly of rings on flat  
240 surfaces (3) and induces inwards/outwards deformations as described earlier. Importantly,  
241 circumferential treadmilling powered by GTP hydrolysis induces an additional torque-twist,  
242 stabilizing smaller ring diameters and supporting further membrane constriction. Regardless  
243 whether protein was externally added or encapsulated, cylindrical geometry allowed clockwise  
244 and anti-clockwise treadmilling (Fig. 5G). Together active FtsZ induces helical transformation  
245 of the membrane tube and a super-constricted state of filaments, imposing a mechanical strain  
246 that promotes breakage and therefore the emergence of treadmilling (Fig. 5F). This establishes  
247 an interesting similarity between FtsZ and dynamin, in which GTP hydrolysis also triggers a  
248 super-constricted state, favoring fragmentation and clustering (19,20). We conclude that these  
249 torques represent a robust constriction mechanism for cylindrically shaped membranes,  
250 generating forces in the range of 0.14-1.09 pN per ring in the case of FtsZ. These FtsZ-induced  
251 forces drive outwards deformations and constriction necks in the case of deflated vesicles *in*  
252 *vitro* and wall-less *E. coli in vivo*. Although the here reported forces do likely not suffice for  
253 the entire process of bacterial cytokinesis of walled rod-like cells, given the temporal relevance  
254 of FtsZ dynamics in the coordination of synthesis of new wall material (5,6), an initial inwards  
255 membrane deformation may be key to trigger cytokinesis, in the form of a “curvature trigger”.

256 In view of our data, we hypothesize that if membrane tension is lowered; for instance, through  
257 the incorporation of de novo synthesized lipids in bacteria septum (10), the here reported force  
258 range might become relevant for the initiation of cell division.

259

## 260 **References:**

- 261 1. T M. Osawa, D. E. Anderson, H. P. Erickson, Reconstitution of Contractile FtsZ Rings in  
262 Liposomes. *Science*. **320**, 792–794 (2008).
- 263 2. M. Osawa, H. P. Erickson, Liposome division by a simple bacterial division machinery.  
264 *PNAS*. **110**, 11000–11004 (2013).
- 265 3. D. A. Ramirez-Diaz *et al.*, Treadmilling analysis reveals new insights into dynamic FtsZ  
266 ring architecture. *PLOS Biology*. **16**, e2004845 (2018).
- 267 4. M. Loose, T. J. Mitchison, The bacterial cell division proteins FtsA and FtsZ self-organize  
268 into dynamic cytoskeletal patterns. *Nat Cell Biol*. **16**, 38–46 (2014).
- 269 5. A. W. Bisson-Filho *et al.*, Treadmilling by FtsZ filaments drives peptidoglycan synthesis  
270 and bacterial cell division. *Science*. **355**, 739–743 (2017).
- 271 6. X. Yang *et al.*, GTPase activity–coupled treadmilling of the bacterial tubulin FtsZ organizes  
272 septal cell wall synthesis. *Science*. **355**, 744–747 (2017).
- 273 7. Holden, S. Probing the mechanistic principles of bacterial cell division with super-  
274 resolution microscopy. *Current Opinion in Microbiology*. **43**, 84–91 (2018).
- 275 8. Coltharp, C. & Xiao, J. Beyond force generation: Why is a dynamic ring of FtsZ polymers  
276 essential for bacterial cytokinesis? *BioEssays*. **39**, e201600179 (2017).
- 277 9. Lan, G., Wolgemuth, C. W. & Sun, S. X. Z-ring force and cell shape during division in rod-  
278 like bacteria. *PNAS*. **104**, 16110–16115 (2007).
- 279 10. Osawa, M. & Erickson, H. P. Turgor Pressure and Possible Constriction Mechanisms in  
280 Bacterial Division. *Front. Microbiol*. **9**, (2018).

- 281 11. A. Roux *et al.*, Membrane curvature controls dynamin polymerization. *PNAS*. **107**, 4141–  
282 4146 (2010).
- 283 12. Krupka, M., Sobrinos-Sanguino, M., Jiménez, M., Rivas, G. & Margolin, W. Escherichia  
284 coli ZipA Organizes FtsZ Polymers into Dynamic Ring-Like Protofilament Structures.  
285 *mBio*. **9**, (2018).
- 286 13. Bassereau, P., Sorre, B. & Lévy, A. Bending lipid membranes: Experiments after W.  
287 Helfrich's model. *Advances in Colloid and Interface Science*. **208**, 47–57 (2014).
- 288 14. D. J. Turner *et al.*, The Mechanics of FtsZ Fibers. *Biophysical Journal*. **102**, 731–738  
289 (2012).
- 290 15. Huecas, S. *et al.* Energetics and Geometry of FtsZ Polymers: Nucleated Self-Assembly of  
291 Single Protofilaments. *Biophysical Journal*. **94**, 1796–1806 (2008).
- 292 16. L. Picas, F. Rico, S. Scheuring, Direct Measurement of the Mechanical Properties of Lipid  
293 Phases in Supported Bilayers. *Biophysical Journal*. **102**, L01–L03 (2012).
- 294 17. Rawicz, W., Olbrich, K. C., McIntosh, T., Needham, D. & Evans, E. Effect of Chain  
295 Length and Unsaturation on Elasticity of Lipid Bilayers. *Biophysical Journal* **79**, 328–339  
296 (2000).
- 297 18. F. Gittes, B. Mickey, J. Nettleton, J. Howard, Flexural rigidity of microtubules and actin  
298 filaments measured from thermal fluctuations in shape. *The Journal of Cell Biology*. **120**,  
299 923–934 (1993).
- 300 19. J. van Mameren, K. C. Vermeulen, F. Gittes, C. F. Schmidt, Leveraging Single Protein  
301 Polymers To Measure Flexural Rigidity. *J. Phys. Chem. B*. **113**, 3837–3844 (2009).
- 302 20. P. Szwedziak, Q. Wang, T. A. M. Bharat, M. Tsim, J. Löwe, Architecture of the ring formed  
303 by the tubulin homologue FtsZ in bacterial cell division. *eLife*. **3**, e04601 (2015).
- 304 21. Arumugam, S. *et al.* Surface Topology Engineering of Membranes for the Mechanical  
305 Investigation of the Tubulin Homologue FtsZ. *Angewandte Chemie International Edition*  
306 **51**, 11858–11862 (2012).

- 307 22. M. Pannuzzo, Z. A. McDargh, M. Deserno, The role of scaffold reshaping and disassembly  
308 in dynamin driven membrane fission. *eLife*. **7**, e39441 (2018).
- 309 23. P. G. de P. Salas *et al.*, Torsion and curvature of FtsZ filaments. *Soft Matter*. **10**, 1977–1986  
310 (2014).
- 311 24. J. Hsin, A. Gopinathan, K. C. Huang, Nucleotide-dependent conformations of FtsZ  
312 dimers and force generation observed through molecular dynamics simulations. *PNAS*. **109**,  
313 9432–9437 (2012).
- 314 25. J. Fierling, A. Johner, I. M. Kulić, H. Mohrbach, M. M. Müller, How bio-filaments twist  
315 membranes. *Soft Matter*. **12**, 5747–5757 (2016).
- 316 26. A. Colom, L. Redondo-Morata, N. Chiaruttini, A. Roux, S. Scheuring, Dynamic remodeling  
317 of the dynamin helix during membrane constriction. *PNAS*. **114**, 5449–5454 (2017).
- 318 27. T. Takeda *et al.*, Dynamic clustering of dynamin-amphiphysin helices regulates membrane  
319 constriction and fission coupled with GTP hydrolysis. *eLife*. **7**, e30246 (2018).
- 320 28. Gao, Y. (2019). Cell division in walled *Bacillus subtilis* and cell wall-lacking *Acholeplasma*  
321 *laidlawii*. PhD thesis, University of Amsterdam.

322

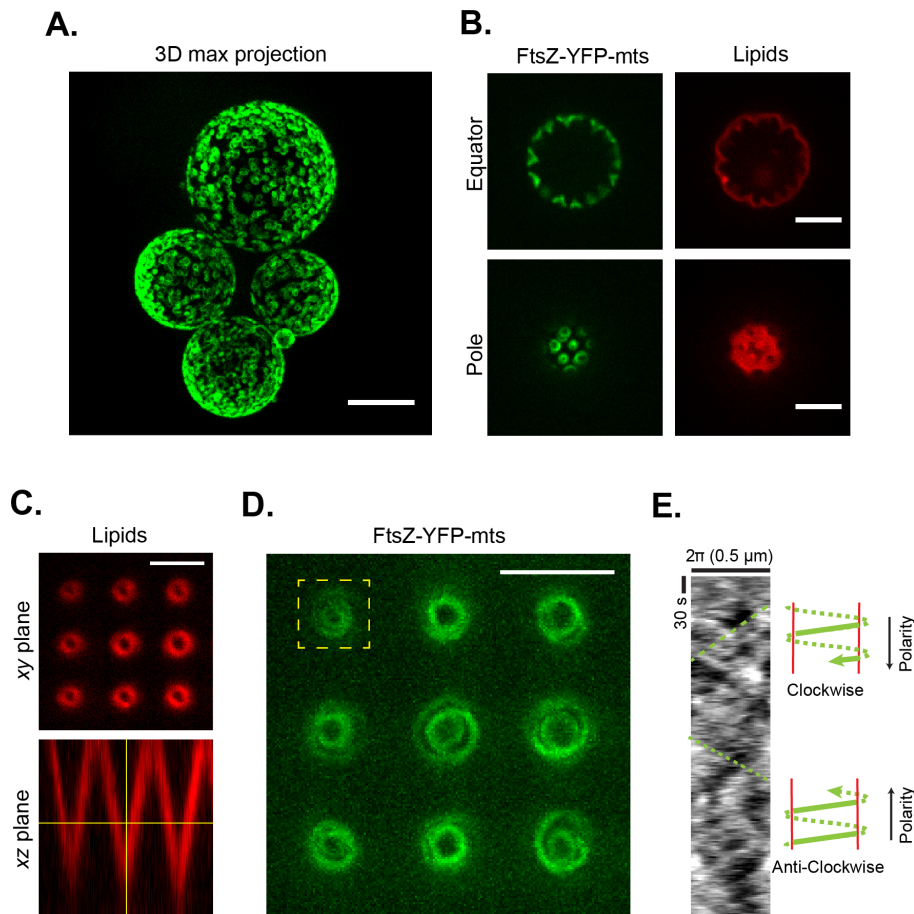
323

324

325 **Acknowledgments:** We acknowledge Dr. Sven Vogel and Dr. Allen Liu for very useful  
326 discussions. We thank MPIB Core Facility for assistance in FtsZ-YFP-mts protein purification.  
327 Funding through MaxSynBio consortium (Federal Ministry of Education and Research of  
328 Germany and the Max Planck Society) grant number 031A359A. The authors have declared  
329 that no competing interests exist. All data is available in the main text or the supplementary  
330 materials.

331

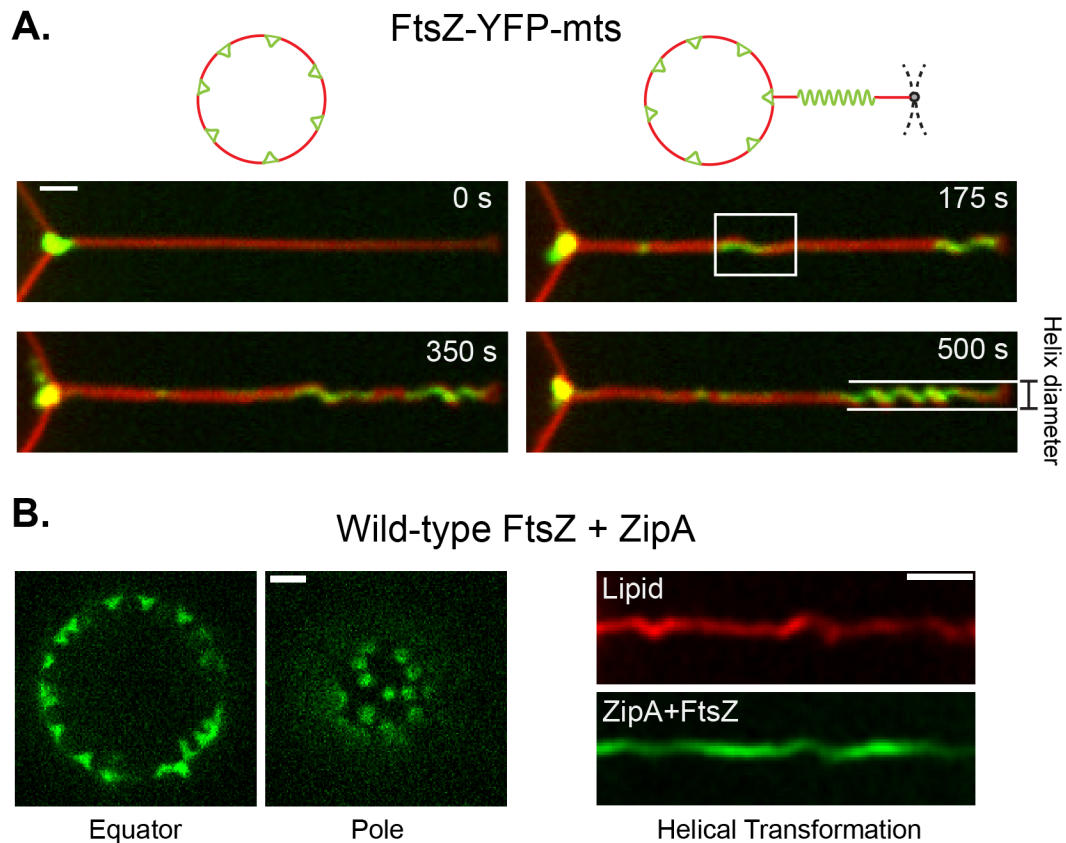
332 **Figure 1.**



333

334 **A)** FtsZ-YFP-mts ring structures externally decorating GUVs (scale bar=10 μm). **B)** After GUV  
335 deflation, inwards conical deformations emerged from FtsZ rings. **C)** Inspired by deformations  
336 in (B), we designed a PDMS microstructure with inwards-conical geometry covered with a  
337 supported lipid bilayer (SLB). The imaging plane was chosen to have a cross-section of ~1 μm  
338 diameter. **D)** Inside cones, FtsZ-YFP-mts self-assembled into dynamic vortices (Movie S1). **E)**  
339 Kymograph showed negative and positive slopes indicating the presence of clockwise and  
340 anticlockwise directions (Scale bar = 5 μm).

341 **Figure 2.**



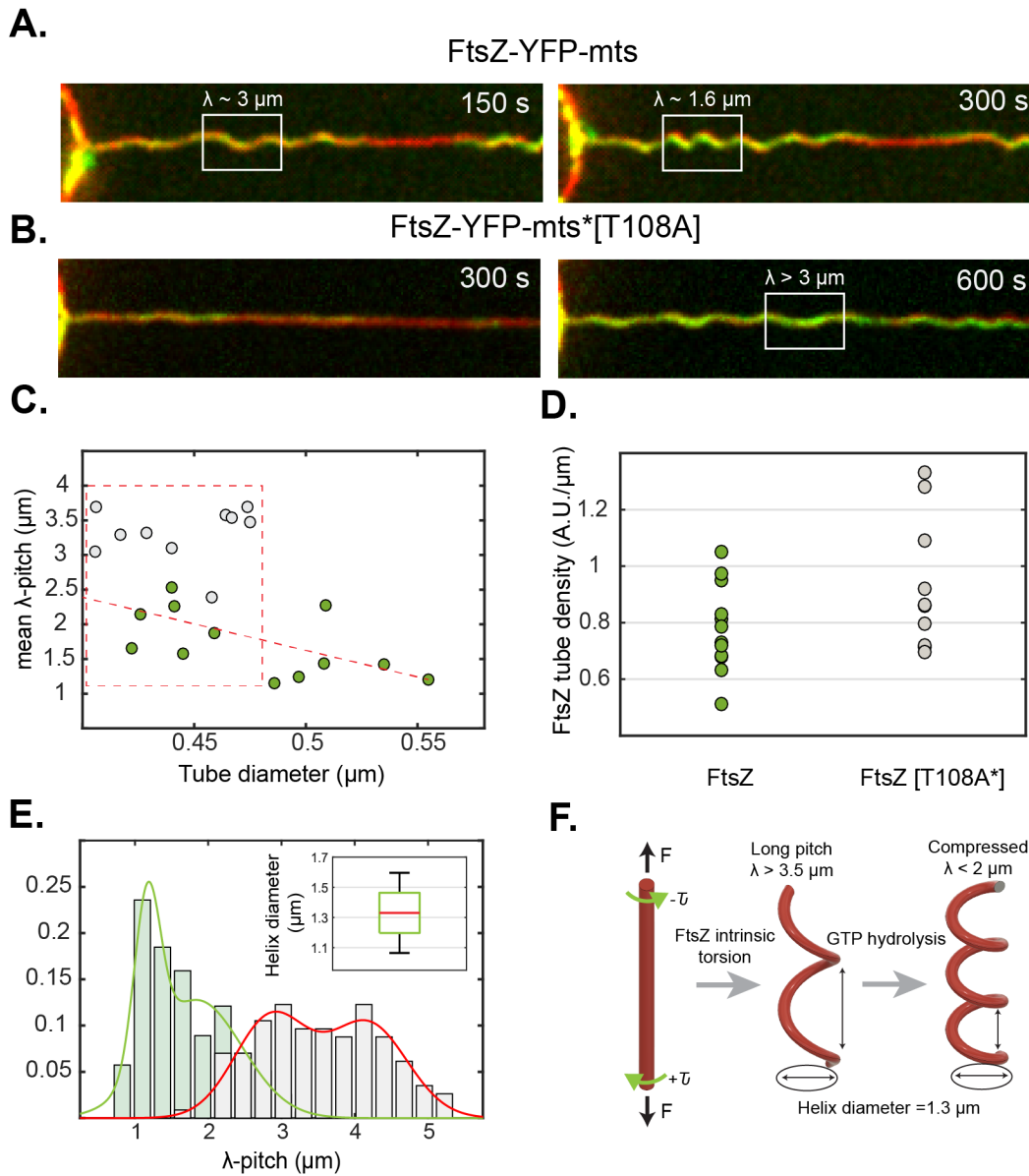
342

343 **A)** To understand inwards deformations, we stretched the cone structures into a tubular  
344 geometry. Soft lipid tubes were pulled from weakly surface-attached GUVs by moving the  
345 GUVs relative to an optically trapped bead. As long as the FtsZ-YFP-mts entered the tube, a  
346 process of coiling is clearly observed as a function of time. As a result, protein being  
347 accumulated over the tip transformed the lipid tube into a spring-like shape. **B)** To rule out that  
348 artificial attachment of the FtsZ-YFP-mts is responsible of the helical transformation, we  
349 reconstituted wild-type FtsZ anchored to the membrane via ZipA to obtain ring-like structures  
350 decorating GUVs. When vesicles were deflated, wild-type FtsZ + ZipA caused inwards cone-  
351 like deformations. After pulling lipid tubes, similar helical deformations were observed  
352 confirming that torsion is related the FtsZ core of the polymer. Fluorescence signal of wt-FtsZ-  
353 Alexa 488 is shown in green while siZipA remains unlabeled. (Scale bar = 2  $\mu$ m).

354

355

356 **Figure 3.**



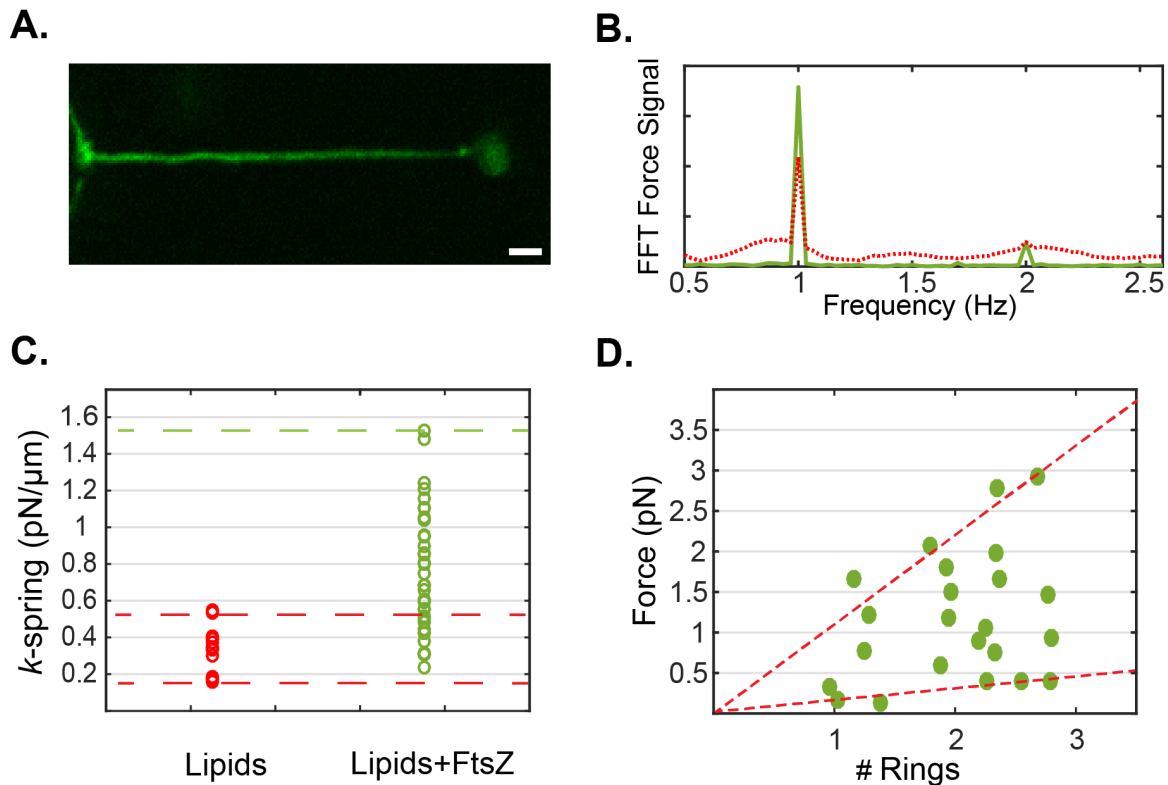
357

358 **A)** FtsZ-YFP-mts and **B)** FtsZ-YFP-mts\*[T108A] promoted helical deformations with the  
 359 difference that GTPase activity induce compression ( $\lambda \sim 1.6 \mu\text{m}$ ) of initially longer pitch ( $\lambda >$   
 360  $3 \mu\text{m}$ ). **C)** To rule out that compression was biased by the deflation state, we plotted tube  
 361 diameter vs mean pitch for FtsZ-YFP-mts (N=12) (green) and FtsZ-YFP-mts\*[T108A] (N=10)  
 362 (gray). Despite of higher tube densities for FtsZ-YFP-mts\*[T108A] as shown in **(D)**, the mean  
 363 pitch for no GTPase case is longer at comparable tube diameters. **E)** We observed two clear  
 364 pitch states for FtsZ-YFP-mts (gray bars/green line) and FtsZ-YFP-mts\*[T108A] (gray bars/red  
 365 line) with a clear dominance of longer pitch for the mutant without GTPase activity. **F)** Helical



366 deformations can be understood by twisting an elastic rod subjected to constant force. We  
367 postulate that FtsZ has an intrinsic torsion that is enhanced by GTPase activity, driving further  
368 compression. Intrinsic FtsZ torsion rules long-pitch transformations ( $\lambda > 3 \mu\text{m}$ ) while GTP  
369 enhances further torsion causing higher pitch states ( $\lambda < 2 \mu\text{m}$ ).

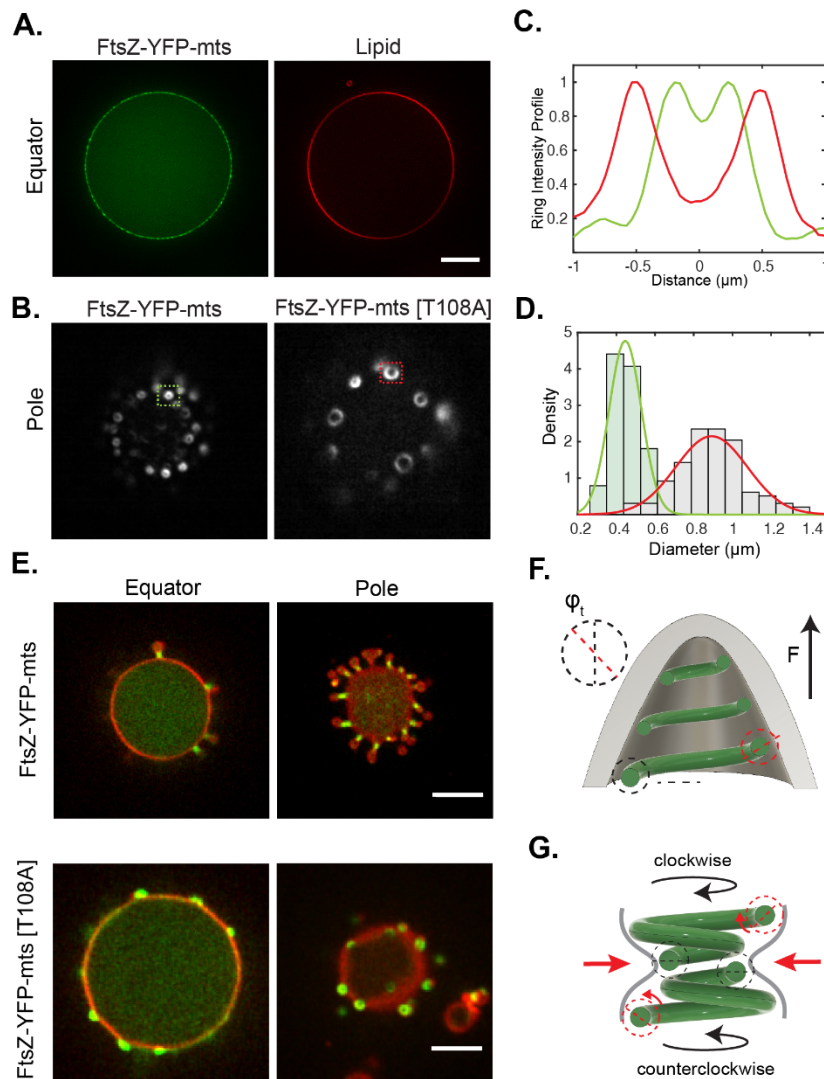
370 **Figure 4.**



371 **A)** Spring-like structures were mechanically assessed by forcing the tube length to oscillate  
372 with an amplitude of  $3 \mu\text{m}$  and a frequency of  $1\text{Hz}$ . **B)** To measure forces, we tracked bead-  
373 displacement as response of the dynamic input. Then, we calculated the Fast Fourier Transform  
374 (FFT) to calculate the amplitude of the signal. Red line: lipid signal and green line: FtsZ. **C)** By  
375 calculating the amplitude, we assessed the spring constant for the case of the only lipid  
376 contribution (N=11) and Lipid+FtsZ (N=36). Dashed red lines indicate the range where the  
377 lipid response dominated over the FtsZ contribution to the spring constant. **D)** By assessing the  
378 average total intensity of FtsZ rings on a flat surface with the same imaging conditions, we  
379 estimated the number of rings for each FtsZ experiments shown in **C)**. Therefore, scattered data  
380

381 representing force vs. number of rings could be described by two dashed red lines with slopes  
382 0.14 and 1.09 pN per ring. These slopes represented the upper and lower limit for the FtsZ  
383 forces per ring.

384 **Figure 5.**



385

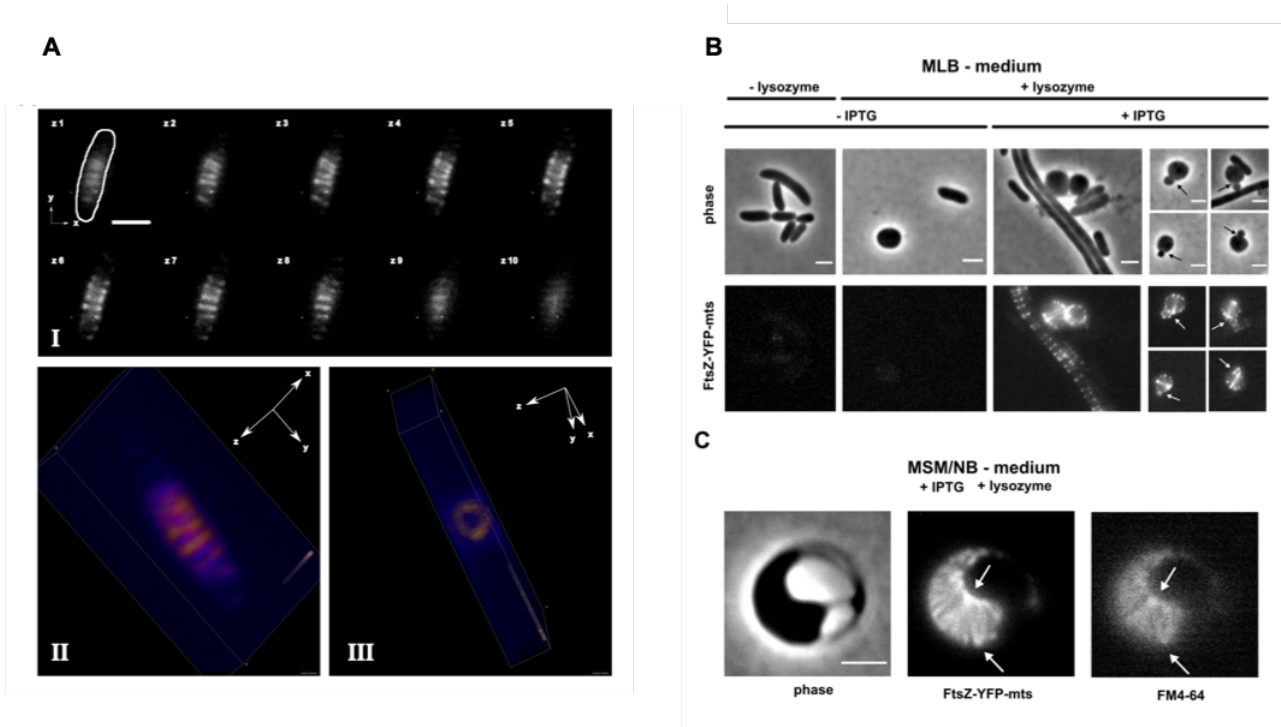
386

387 **A)** FtsZ-YFP-mts and FtsZ-YFP-mts\*[T108A] rings inside GUVs. **B)** Imaging of rings, at  
388 GUVs bottom, using TIRF microscopy. **C)** Intensity profile of structures indicated in (B)  
389 showed that FtsZ-YFP-mts (green line) rings exhibit smaller diameter than FtsZ-YFP-  
390 mts\*[T108A] (red line). **D)** Size distribution of (N=112) FtsZ-YFP-mts\*[T108A] (gray bars  
391 and red line) and (N=102) FtsZ-YFP-mts showed a drastic reduction in ring diameter due to

392 GTP hydrolysis. **E)** After deflation, both mutants drove outwards deformations with the  
393 difference that GTPase activity promotes constriction and neck formation. **F)** We suggest that  
394 intrinsic torsion can create out-of-plane forces; however, **G)** GTP hydrolysis triggered a super-  
395 constricted state favoring higher curvatures.

396

397 **Figure 6.**



398 **A)** *E. coli* DH5 $\alpha$  cells expressing FtsZ-YFP-mts polymeric structures perpendicular to the cell  
399 diameter around midcell (AI). 3D rendering reveals ring-like structures (AII-AIII). **B)** Removal  
400 of the cell wall by lysozyme treatment leads to spheroplast formation. Expression of FtsZ-YFP-  
401 mts leads to membrane vesiculation (arrows). **C)** Sphaeroplasts expressing FtsZ-YFP-mts show  
402 drastic deformations of the plasma membrane. FtsZ assemblies lead to local membrane  
403 invaginations (white arrows), indicating force generation. Scale bars 2  $\mu$ m.

404

405

406

407

408 **Code availability**

409 All custom code is available on request.

410 **Data availability**

411 All data are available in the main text, the supplementary materials, or upon request.

412